Electronic noise in a GaAs/AlGaAs Heterojunction with a graded barriers

P. K. D. D. P. Pitigala[1,2*], A.G.U. Perera[2]

[1]*Department of Physics, University of Sri Jayewardenepura, Gangodavila, Nugegoda.*
[2]*Department of Physics and Astronomy, Georgia State University, Atlanta, GA 30303*
dpitigala@sjp.ac.lk

ABSTRACT

The noise spectra was measured and analyzed, of a heterojunction structures, with a GaAs emitter sandwiched between two AlGaAs barriers. One of the barriers here was slanted (graded) by gradually changing the aluminum fraction, whilst the second barrier was kept flat (constant). A structure, with both barriers are flat, was used as the control sample. Results show the presence of different noise components such as the generation–recombination (G-R), 1/f, Johnson, and Shot noise in both devices. Taken as total and as individual components, the lowest noise spectra were observed for the flat barrier device. The high noise in the graded barrier device is attributed to the high dark current resulted by low internal resistance in the structure and the two G-R noise sources were identified as the deep traps (at ~0.54 eV and ~0.39 eV above the valence band of AlGaAs) possibly resulted by do pant migration and defects.

1. INTRODUCTION

Different types of noise, both internal and external, are observed in many optoelectronic devices. External noise is generated by outside sources such as power supply units, amplifiers and antenna effects in connecting wires and leads to the device. Internal noise can be generated by the device's material properties[1] and structure[2-4].Many of the common noise sources are uncorrelated, and therefore can be summed, with the noise spectrum being a primary limitation to, and often significantly degrading the performance of optoelectronic devices. Low noise is thus one of the principal requirements for obtaining a higher detectivity (D*) in infrared photo detectors, making it essential to study and identify the origins of all noise source.

Internal noise is mainly generated by dark currents, temperature fluctuations, and trap states in the structures. Material quality and the device structure could also play a role in noise generation .When an electrical current passes through a material, fluctuation in the current give rise to shot noise. Fluctuations in thermal motion of charged particles due to temperature and resistance result in Johnson noise. Both are independent of frequency, and are known as "white noise". Scattering and trapping of carriers leads to generation-recombination (G-R) noise, and are principally observed in photoconductors. G-R noise can increase with the trap density in the material. 1/f, or flicker noise is the least understood noise source, inversely proportional to the frequency.

High noise values have been reported for AlGaAs based bipolar transistors [5, 6]. This

has been attributed to a high volume resistance, combined with a large space charge region, which leads to trapping of carriers, and hence an increase in the G-R noise density. Highly doped emitters can also lead to excess noise owing to traps formed by clustering of impurities[7]. Such effects decrease the gain of optoelectronic devices.

Split-off band detectors based on GaAs/AlGaAs heterostructures are recently demonstrated as an un cooled infrared detector[8]. Split-off band infrared detectors works based on the carrier transiting in heavy hole / light hole bands and split-off band in the p-doped material.[8, 9] Implementation of graded barriers have been proposed for p-type split-off band infrared detectors [10] to improve their responsivity and detectivity. The noise generated in such a device plays a major role, because the detectivity is inversely proportional to the square root of the noise power of the device. Therefore, understanding the effects on the device noise with implementation of the graded barrier is essential.

2. DEVICE STRUCTURES AND EXPERIMENTAL PROCEDURE

Two structures are used in the study, and the device parameters are shown in Table 1. The structures were grown using the molecular beam epitaxy, the graded barrier was constructed by changing the aluminum concentration with time. Out of the two, one stricture has a graded barrier, and the other structure has a constant barrier in place of the graded barrier and is used as the control. Schematic of the valence band alignment of the graded barrier structure and the constant barrier structure is shown in the Fig. 1(a) and (b) respectively. All the structures have a highly p-doped ($1x10^{19}$ cm^{-3}) emitter sandwiched between the two AlGaAs barriers. The width of the graded barrier was set to 80 nm while the constant barrier width is 400 nm. The emitter thickensis 80 nm for both the devices. To construct the graded barrier, the aluminum fraction was changed gradually from (X_1) 45% to (X_2) 75% by adjusting the substrate temperatures and aluminum flow during the growth.

Table 1: Device structure details with different aluminum fractions in. X_1, X_2, and X_3 corresponding the positions marked in Figure 1. All emitters are highly p-doped to 1×10^{19} cm^{-3}.

Device label.	Lower Edge Al% (h_1)	Higher Edge Al% (h_2)	Constant Barrier Al% (h_3)	Emitter thickness (W)
1001	0.75	0.75	0.57	80 nm
1007	0.45	0.75	0.57	80 nm

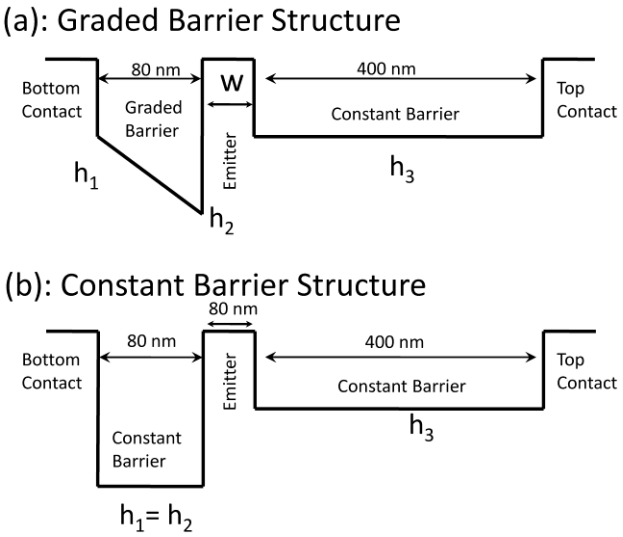

Figure 1: Schematic of the valence band diagram of the devices: (a) the graded barrier and (b) the constant barrier structure. The barrier thicknesses are 80nm and 400nm, and the emitter is 80 nm. Al fractions (h_i) are tabulated in Table 1.

Noise current densities were measured using the Stanford Research System (SR785) dynamic signal analyzer connected through an SR-570, low noise current amplifier to the sample. Each device was biased with a voltage of -50 mV, using the internal biasing in the SR-570. The capacitance-voltage measurements of the devices were measured usingan HP 4284A LCR meter, and a closed cycle refrigerator is used for temperature variant.

The modeling data was calculated from equation 1 [6],where A, and A_j are constants, I is the dark current at the given bias voltage, f is the frequency, and f_j is the cut-off frequency of each generation-recombination (G-R) noise component.

$$S(f) = \frac{AI^2}{f} + \sum_j \frac{A_j I^2}{\left(1 + \frac{f}{f_j}\right)} + 2qI + \frac{4K_B T}{R} \qquad (1)$$

The first term in the equation represents the 1/f noise in the device, and the second term represents the G-R noise components. The last two terms are the shot and Johnson noise of the device, due to the dark current and thermal resistivity fluctuations respectively. In Eq. (1), q is the charge of an electron, k_B is the Boltzmann constant, T is the absolute temperature, and R is the resistance of the device.

The trap energy level was calculated from the equation 2 [6]where E_T is the hole trap level energy (measured to the valence band), σ the capture cross section, ν the thermal velocity, N the density of states in the majority carrier band, and τ the time constant.

$$E_T = k_B T \, Ln\left(\frac{2\sigma\vartheta N}{\tau}\right) \quad (2)$$

3. RESULTS & DISCUSSION

3.1 The electronic noise in the devices

The noise power S(f) under the 50 mV bias for the devices 1001 and 1007 are shown in Fig. 2(a) and (b), respectively. The Dashed and dotted lines represents the 1/f component and the G-R noise component in each device extracted from the Eq. 1. The solid thick curve represents the sum of all noise components as represented by Eq. 1. The dip seen at the high frequencies in the Fig. 2(a) is due to limitation in the signal amplifier at high sensitivity settings, required due to low noise power observed in 1001 compared to 1007. The lowering sensitivity setting in the amplifier makes it difficult to identify the G-R noise component in the 1001 device.

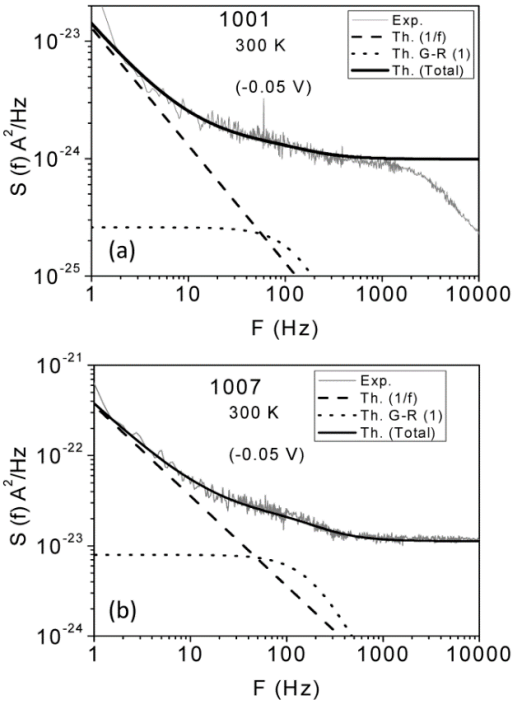

Figure 2. The noise power (S_f) of the devices (a) 1001 and (b) 1007 under constant bias of -50mV (Under the negative bias the hole current is from top contact to bottom contact). The dashed and dotted curves represent the 1/f component and the G-R noise component in each device decomposed according to Eq. 1.

3.2 Decomposition of the noise components

The measured noise current density, are decomposed to the different noise components as stated by different terms in Eq. 1 as illustrated in Fig.2.The calculated curve (Th. Total) is the sum of all four noise components and the constants A, and A_j were selected to match the amplitude of the calculated curve to the measured noise spectrum. The value of f_i is chosen so that the inflection in the measured spectrum is replicated in the calculated curve. It clearly shows that the calculated spectrum lies well within the uncertainty in the experimental results.

3.2.1 1/f noise

As shown in Fig. 2, in 1001, 1/f noise dominates in low frequency range up to ~20 Hz, and extends up to ~ 30 Hz for the 1007.And the dark current and temperature dependent shot and Johnson noise dominates at higher frequencies. The α factor in $1/f^{\alpha}$ noise laid around 1±0.1 for both the devices. And as the bias increase in both the negative and positive bias the α varies from 0.8 to 1.5.

3.2.2 G-R noise

The G-R noise component (G-R (1)) is appearing in the range from ~30 Hz to ~500 Hz. The domination of the Shot and Johnson noise can result in shadowing some of the weak G-R noise signals. (In section 4 few additional traps were identified, which can be G-R noise sources, but are not clearly shown in the noise spectra)The G-R(1) has its characteristic frequency at 50 ± 10 Hz, which gives a time constant of ~ 3.2 ± 0.7ms.This frequency corresponds to a trap level at 0.54 ± 0.01eV above the valence band (VB), which is in the range of the reported hole trap levels at 0.54 eV, for both beryllium doped and undoped films of GaAs[11, 12].

Additionally a signal corresponds to a second G-R component (G-R (2)) was observed, mainly in 1007with a characteristic frequency of 16.5 ± 1.5 kHz, corresponding to a trap level at 0.390 ± 0.005 eV above the valence band (VB). Even though a clear cut-off frequency (a hump) is not clearly visible in the measured noise spectrum, a second G-R noise component has to be added to the calculated noise spectrum in order to be in agreement with the experimental spectrum. The energy correspond to the G-R (2) agrees with the hole trap level reported in the literature at 0.4 eV for beryllium doped AlGaAs films [13, 14].This implies possible dopants migration into the barrier layers from the highly doped emitters. The C-V data confirms the existence of the traps at 0.39 eV and 0.53 eV which closely agrees with the G-R noise observed in the devises.

Considering the plateau level of G-R (1) noise components in Fig.2, the lowest G-R noise levels are observed in the structure with the flat barrier (1001). The two possible reasons for this observation is the higher density of traps may be generated at the AlGaAs barrier in 1007 due to the varying aluminum content while growth. Additionally there can be a higher doping migration into the barriers, as the aluminum fraction at the one edge of the 1007 is low; hence the properties are much closer to the GaAs, but the AlGaAs. Furthermore, it can be a result of beryllium doped GaAs layers itself as there can be a large variation in trap states in beryllium doped GaAs layer as a variation in hole trap densities from $8\times10^{12}cm^{-3}$ to 1.6×10^{14} cm^{-3} has been observed[15].

3.2.3 Shot and Johnson noise

As expected, by observing the high dark current and the change of the device dynamic resistance the Shot and Johnson noise in the constant barrier structure is lower than the respective noise levels in the graded barrier structures.

3.3 Extracting the Trap level energies in the devices

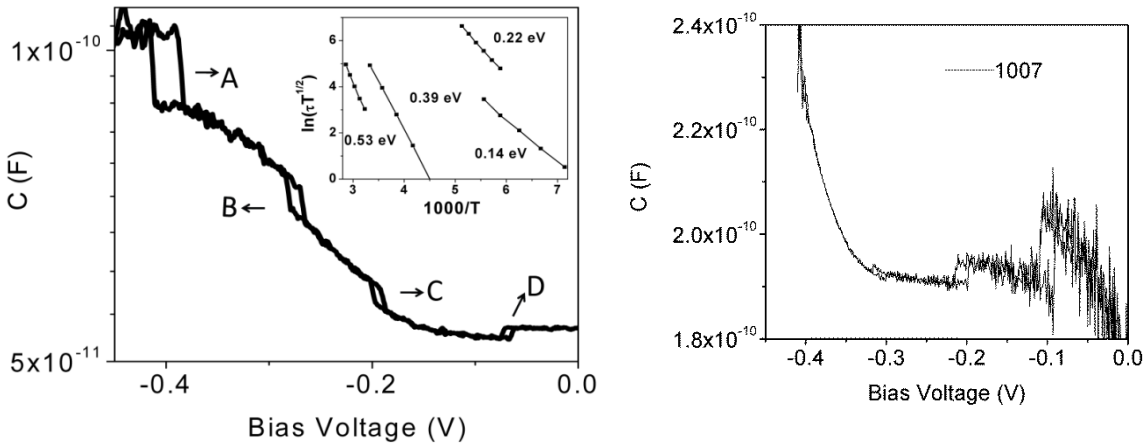

Figure 3: The C-V scan for 1001 and 1007. Both the devices show hysteresis in the capacitance, due to the existence of a trap in the materials. Four hysteresis loops (A, B, C, and D) were observed. Inset: The Arrhenius plot of time constant vs 1/T for devices. The Arrhenius plot reveals trap energy levels at 0.53 ± 0.01 eV, 0.36 ± 0.02 eV, 0.22 ± 0.04 eV and 0.14 ± 0.02 eV.

Table 2: Observed trap levels and the corresponding trap states as reported in literature.

Observed Trap Energy (eV)	**Traps reported in Literature (close to observed traps)**		
	Material	**Energy Level (eV)**	**Origin of the Trap according to literature**
0.53	AlGaAs	0.55	Cu[16]
	GaAs	0.54	Unknown [8-9]
	GaAs	0.52	Fe[17]
0.5	AlGaAs	0.46	Unknown [13]
	GaAs	0.44	Cu[17]
0.39	AlGaAs	0.4	Unknown [13, 14]
0.22	AlGaAs	0.3	Unknown [16]
	GaAs	0.29	Ga vacancy [14]
0.14	GaAs	0.14	Unknown [13]

The capacitance-voltage (C-V) trace of the two devices shows a hysteresis in the capacitance, confirming the existence of a trap level. The C-V scan for 1001 is shown in figure 3. Four hysteresis loops (named as A, B, C, and D) were observed, and the hysteresis can be explained by the following mechanism. At zero bias the trap states will be empty and the Fermi level will lie below the traps. When sweeping the bias voltage, the Fermi level will sweep above the trap states and the trap states will be filled, hence changing the capacitance. When sweeping the bias voltage down, the Fermi level will fall below the trap state but, to empty the filled traps, a much higher voltage difference is required. Therefore, the step in the capacitance will occur at a different voltage, resulting hysteresis in the C-V sweep.

The Arrhenius plots, of the time constant acquired from the C-V sweeps, are shown in the inset of figure 3; reveals trap energy levels at 0.53 ± 0.01 eV and 0.39 ± 0.02 eV, confirming the two trap levels responsible for the G-R noise. Additional trap levels were also observed and the corresponding trap levels reported in the literature with possible cause for the traps according to literature are summarized in Table 2.

4. CONCLUSION

In conclusion, the electronic noise in a (graded)AlGaAs/GaAs/(constant)AlGaAs structures were tested. A higher shot noise and Johnson noise power density is observed for the devices with the graded barrier, compared to the control sample, the structure with the two constant AlGaAs barriers. Additionally, two G-R noise components were observed in the device with the graded AlGaAs barrier, whilst other only show the presence of one G-R noise component. Even though, four trap levels have been identified in each device through C-V measurements, the noise data have not shown a clear signature of existence of four G-R noise components. It assumes the low trap densities and limitations in the instruments have resulted in such an observation. The discrepancy in the shot noise and the Johnson noise is attributed to the dark current and the internal device resistance. The low dark current and high device resistance reduces the noise power of constant barrier devices. The lowest noise levels in all devices are present at frequencies higher than 500 Hz; therefore to achieve higher D* in photon detection applications a modulation frequency of 500 Hz or above should be used.

5. ACKNOWLEDGEMENTS

A special thank goes to Prof. E H Linfield at University of Leeds for providing the samples for this study.

6. REFERENCES

[1] Ershov, M., Korotkov, A.N., Noise in single quantum well infrared photodetectors, Applied Physics Letters 71 (1997) 1667-1669.

[2] Rupani, R.A., Ghosh, S., Su, X., Bhattacharya, P., Low frequency noise spectroscopy in InAs/GaAs resonant tunneling quantum dot infrared photodetectors, Microelectronics Journal 39 (2008) 307-313.

[3] Pitigala, P.K.D.D.P., Jayaweera, P.V.V., Matsik, S.G., Perera, A.G.U., Liu, H.C., Highly sensitive GaAs/AlGaAs heterojunction bolometer, Sensors and Actuators A: Physical 167 (2011) 245-248.

[4] Perera, A.G.U., Shen, W.Z., Ershov, M., Liu, H.C., Buchanan, M., Gunapala, S.D., Bandara, S.V., Liu, J.K., Ye, H.H., Schaff, W.J., Effect of interface states on the performance of GaAs p[sup +]-i far-infrared detectors, AVS, Ottawa, Canada, 2000, pp. 597-600.

[5] Kleinpenning, T.G.M., Holden, A.J., 1/f noise in n-p-n GaAs/AlGaAs heterojunction bipolar transistors:iImpact of intrinsic transistor and parasitic series resistances, Electron Devices, IEEE Transactions on 40 (1993) 1148-1153.

[6] Pascal, F., Jarrix, S., Delseny, C., Lecoy, G., Kleinpenning, T., Generation-recombination noise analysis in heavily doped p-type GaAs transmission line models, Journal of Applied Physics 79 (1996) 3046-3052.

[7] Makinen, J., Corbel, C., Hautojarvi, P., Moser, P., Pierre, F., Positron trapping at vacancies in electron-irradiated Si at low temperatures, Physical Review B 39 (1989) 10162.

[8] Jayaweera, P.V.V., Matsik, S.G., Perera, A.G.U., Liu, H.C., Buchanan, M., Wasilewski, Z.R., Uncooled infrared detectors for 3--5 mu m and beyond, Applied Physics Letters 93 (2008) 021105-021103.

[9] Lao, Y.F., Pitigala, P.K.D.D.P., Perera, A.G.U., Liu, H.C., Buchanan, M., Wasilewski, Z.R., Choi, K.K., Wijewarnasuriya, P., Light-hole and heavy-hole transitions for high-temperature long-wavelength infrared detection, Applied Physics Letters 97 (2010) 091104-091103.

[10] Matsik, S.G., Jayaweera, P.V.V., Perera, A.G.U., Choi, K.K., Wijewarnasuriya, P., Device modeling for split-off band detectors, Journal of Applied Physics 106 (2009) 064503-064506.

[11] Brammertz, G., Martens, K., Sioncke, S., Delabie, A., Caymax, M., Meuris, M., Heyns, M., Characteristic trapping lifetime and capacitance-voltage measurements of GaAs metal-oxide-semiconductor structures, Applied Physics Letters 91 (2007) 133510-133513.

[12] Lagowski, J., Gatos, H.C., Parsey, J.M., Wada, K., Kaminska, M., Walukiewicz, W., Origin of the 0.82-eV electron trap in GaAs and its annihilation by shallow donors, Applied Physics Letters 40 (1982) 342-344.

[13] Szatkowski, J., Placzek-Popko, E., Sieranski, K., Hansen, O.P., Deep hole traps in Be-doped Al[sub 0.5]Ga[sub 0.5]As layers grown by molecular beam epitaxy, Journal of Applied Physics 86 (1999) 1433-1438.

[14] Mari, R.H., Shafi, M., Aziz, M., Khatab, A., Taylor, D., Henini, M., Electrical characterisation of deep level defects in Be-doped AlGaAs grown on (100) and (311)A GaAs substrates by MBE, Nanoscale Research Letters 6 (2011) 180.

[15] Bhattacharya, P.K., Buhlmann, H.J., Ilegems, M., Staehli, J.L., Impurity and defect levels in beryllium-doped GaAs grown by molecular beam epitaxy, Journal of Applied Physics 53 (1982) 6391-6398.

[16] Szatkowski, J., Sieranski, K., Hajdusianek, A., Placzek-Popko, E., Deep hole traps in Be-doped Al0.2Ga0.8As layers grown by molecular beam epitaxy, Physica B: Condensed Matter 340-342 (2003) 345-348.

[17] Ilegems, M., Properties of III-V layers, in: Parker, E.H.C. (Ed.), The Technology and Physics of Moleculer Beam Epitaxy, Plenum Press, New York and London, 1985, pp. 83-142.